PHYSICAL REVIEW B **92**, 041104(R) (2015)

Anisotropic magnetotransport and exotic longitudinal linear magnetoresistance in WTe_2 crystals

Yanfei Zhao,[1,2] Haiwen Liu,[1,2] Jiaqiang Yan,[3,4] Wei An,[2,5] Jun Liu,[6] Xi Zhang,[1,2] Huichao Wang,[1,2] Yi Liu,[1,2] Hua Jiang,[7] Qing Li,[8] Yong Wang,[6] Xin-Zheng Li,[2,5] David Mandrus,[3,4] X. C. Xie,[1,2] Minghu Pan,[9,*] and Jian Wang[1,2,†]

[1]*International Center for Quantum Materials, School of Physics, Peking University, Beijing 100871, China*

[2]*Collaborative Innovation Center of Quantum Matter, Beijing 100871, China*

[3]*Department of Materials Science and Engineering, University of Tennessee, Knoxville, Tennessee 37996, USA*

[4]*Materials Science and Technology Division, Oak Ridge National Laboratory, Oak Ridge, Tennessee 37831, USA*

[5]*School of Physics, Peking University, Beijing 100871, China*

[6]*Center of Electron Microscopy, State Key Laboratory of Silicon Materials, Department of Materials Science and Engineering, Zhejiang University, Hangzhou, 310027, China*

[7]*College of Physics, Optoelectronics and Energy, Soochow University, Suzhou 215006, China*

[8]*Institute of Functional Nano and Soft Materials (FUNSOM) and Collaborative Innovation Center of Suzhou Science and Technology, Soochow University, Jiangsu 215123, China*

[9]*MOE Key Laboratory of Fundamental Physical Quantities Measurements, School of Physics, Huazhong University of Science and Technology, Wuhan 430074, China*

(Received 16 February 2015; revised manuscript received 11 June 2015; published 6 July 2015)

The WTe_2 semimetal, as a typical layered transition-metal dichalcogenide, has recently attracted much attention due to an extremely large, nonsaturating parabolic magnetoresistance in the perpendicular field. Here, we report a systematic study of the angular dependence of the magnetoresistance in a WTe_2 single crystal. The significant anisotropic magnetotransport behavior in different magnetic field directions and violation of the Kohler's rule are observed. Unexpectedly, when the applied field and excitation current are both parallel to the tungsten chains of WTe_2, an exotic large longitudinal linear magnetoresistance as high as 1200% at 15 T and 2 K is identified. Our results imply that the WTe_2 semimetal, due to its balanced hole and electron populations, seems to be the first material for which a large longitudinal linear magnetoresistance appears when the external magnetic field is parallel to the applied current. Our work may stimulate studies of double-carrier correlated materials and the corresponding quantum physics.

DOI: 10.1103/PhysRevB.92.041104 PACS number(s): 72.15.Eb, 72.15.Gd, 72.80.Ga, 75.47.−m

In contrast to classical quadratic magnetoresistance (MR) in metals and semiconductors, linear magnetoresistance (LMR) is an unusual phenomenon in condensed matter. LMR has been found only in limited materials, including silver chalcogenides [1], multilayer epitaxial graphene [2], topological insulators [3–5], and three-dimensional Dirac semimetals such as Cd_3As_2 [6–8] and TlBiSSe [9], and has often been interpreted by either the theory proposed by Abrikosov [10] or the inhomogeneity in materials [1]. LMR behaviors are usually observed in a magnetic field applied perpendicular to the direction of the excitation current and have become one of the significant research interests in condensed matter physics and material science.

Semimetal tungsten ditelluride (WTe_2), due to its extremely large, nonsaturating magnetoresistance, has attracted significant research interest recently [11–17]. WTe_2 is a typical layered transition-metal dichalcogenide (TMD) with tungsten chains sandwiched by adjacent chalcogenide layers. The extremely small overlap between the bottom of the conduction band and the top of the valence band in WTe_2 results in many interesting properties, such as a complicated band structure with multiple Fermi pockets [11,12], an extremely large MR effect reaching 1.3×10^7% at 60 T and 0.53 K in the perpendicular field [11], pressure-induced superconductivity [15,16], and a predicted potential topological property [17]. However, a detailed angle-dependent MR study, representing the anisotropic properties of WTe_2, has not been fully investigated and still remains unclear.

In this Rapid Communication, we report a systematic study to reveal the anisotropic transport behavior in a WTe_2 single crystal. A large residual resistance ratio (RRR) of 741 in zero field and a significant anisotropic resistivity as well as anisotropic magnetotransport behavior in different magnetic field directions are observed. Strikingly, when the applied magnetic field is parallel to the excitation current along the tungsten chains (*a* axis) of WTe_2, an exotic large longitudinal LMR as high as 1200% at 15 T and 2 K is identified. Our results suggest that, due to its balanced hole and electron populations, WTe_2 may be the first material for which a longitudinal LMR appears when the magnetic field is applied parallel to the applied current.

W and Te shots in an atomic ratio of 1 : 49 were placed in a 5 ml Al_2O_3 crucible to grow WTe_2 single crystals. A catch crucible containing quartz wool was mounted on top of the growth crucible and both were sealed in a silica ampoule under approximately 1/3 atmosphere of high pure argon gas. The sealed ampoule was heated up initially to 1100 °C and kept for 6 h, then cooled down to 500 °C over 96 h. The Te flux was separated from the single crystals by using a centrifuge once the temperature reached 500 °C. The WTe_2 single crystal grown by this method, further studied by a FEI Tecnai F20 transmission electron microscope operated at 200 kV, was proven to be of high quality. Figure 1(a) shows an atomically high-resolution transmission electron microscopy

*Corresponding author: mhupan@gmail.com

†Corresponding author: jianwangphysics@pku.edu.cn

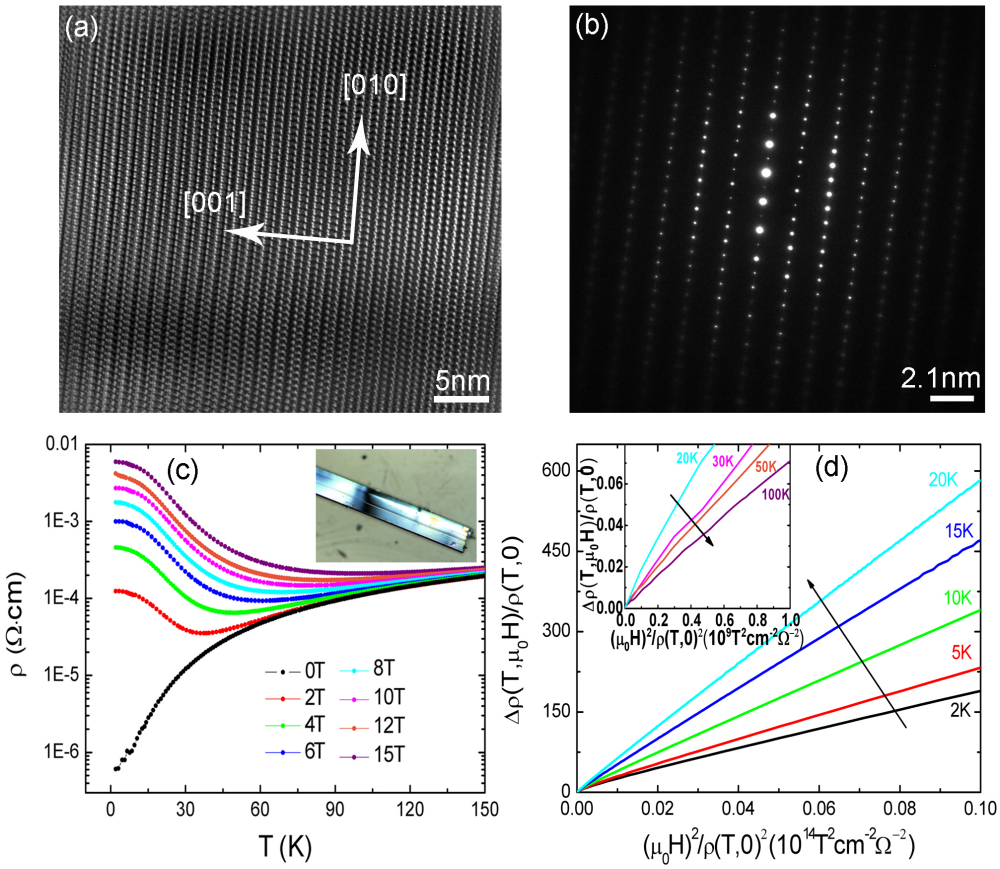

FIG. 1. (Color online) (a) High-resolution transmission electron microscopy image of the WTe_2 single crystal. (b) Electron diffraction image looking down the [100] zone axis showing the reciprocal lattice of WTe_2. (c) Temperature dependence of longitudinal ρ of WTe_2 (sample 1) at different perpendicular magnetic fields. Inset: Optical image of the WTe_2 single crystal. (d) Kohler's rule by plotting the $\rho(T,\mu_0H)/\rho(T,0)$ vs $(\mu_0H)^2/\rho(T,0)^2$ from 2 to 20 K. The inset shows the high temperature regime from 20 to 100 K.

(HRTEM) image, suggesting crystal growth preferentially along the [001] direction (c axis). Figure 1(b) shows the selected area electron diffraction (SAED) pattern looking down the [100] zone, further indicating the single crystal structure of WTe_2. Both the HRTEM image and SAED pattern of our samples [Figs. 1(a) and 1(b)] show that the crystal lattice measurements are $c = 1.401$ nm and $b = 0.625$ nm, which are the same measurements as a previously reported WTe_2 single crystal structure [18,19]. Furthermore, the energy dispersive spectrometer (EDS) experimental result confirms the stoichiometric WTe_2 (shown in the Supplemental Material [20]).

An optical image of a typical WTe_2 single crystal for transport measurements is shown in the inset of Fig. 1(c). The transport results reported here are primarily from sample 1 with a size of ~1.5 mm × 0.2 mm × 15 μm (length × width × thickness). The standard four-electrode method was used for the measurements and the current was applied along the tungsten chains (a axis). Figure 1(c) shows the resistivity as a function of temperature at different magnetic fields, which are perpendicular to the chalcogenide layers (along the c axis). With decreasing temperature, the resistivity exhibits a well-metallic behavior at zero field by showing a huge residual resistance ratio (RRR = 741), much larger than the reported values in other semimetals such as Bi [21] and $NbSb_2$ [22]. Interestingly, when applying the magnetic field, the resistivity displays a remarkable increase in the low temperature regime showing a metal-insulator transition [23]. Figure 1(d) shows the Kohler's analysis of the resistivity curves at various temperatures. According to Kohler's theory [24],

$$\frac{\Delta\rho(T,\mu_0H)}{\rho(T,0)} = F\left(\frac{\mu_0H}{\rho(T,0)}\right), \tag{1}$$

where ρ is the resistivity, T is the temperature, and H is the magnetic field. If the carrier density of the system is robust to temperature variation, the MR measured at different temperatures can be scaled into a single curve. Here, we assume the function $F(\frac{\mu_0H}{\rho(T,0)}) = A(T)(\frac{\mu_0H}{\rho(T,0)})^2$ in the perpendicular field with a parameter $A(T)$, due to the parabolic dependence of the magnetic field at different temperatures when $H \parallel c$ axis. As shown in Fig. 1(d), the scaled MR curves deviate from the Kohler's rule with $A(T)$ changes with temperature, and the temperature effect is analyzed in the following.

Figure 2 shows the normalized MR $[\rho(H)/\rho(0)]$ of WTe_2 measured in different field directions at various temperatures. The schematic structure for the magnetotransport measurements is shown in Fig. 2(a). The current is applied along the a axis. In the perpendicular field ($H \parallel c$ axis) configuration, as shown in Fig. 2(b), pronounced Shubnikov–de Haas (SdH) oscillations are clearly visible around 5 T at 2 K. The MR reaches as high as 1.1322×10^6% at 14.7 T and 2 K, about three times larger than previously reported values [11,14]. With

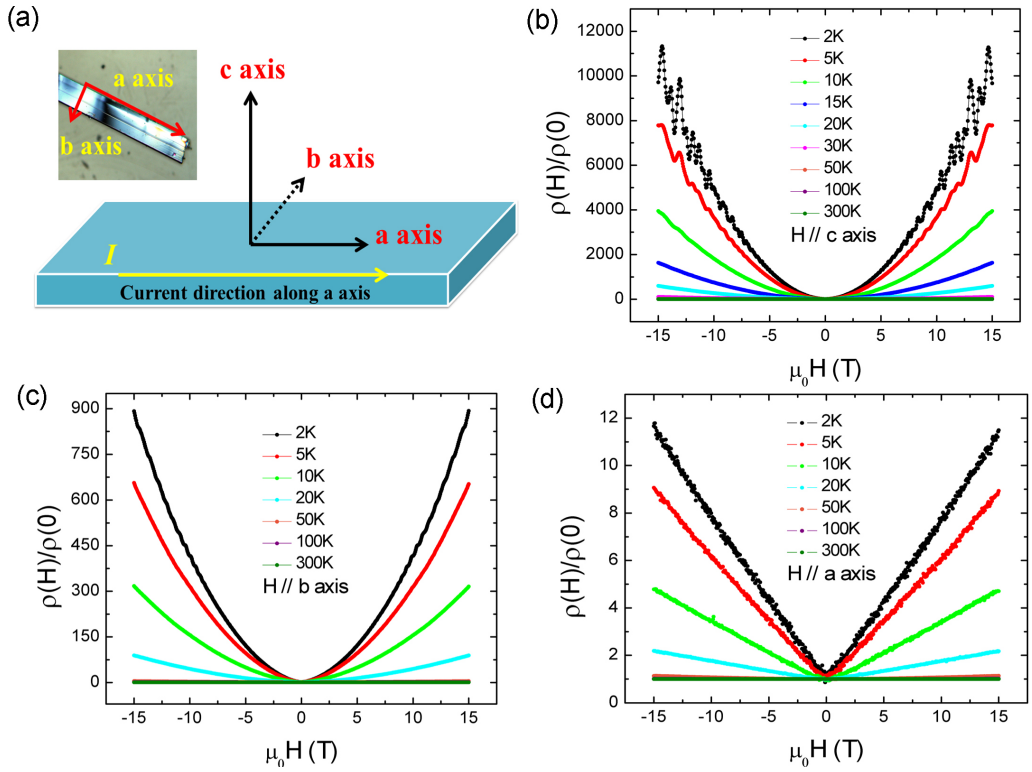

FIG. 2. (Color online) (a) Schematic structure for the magnetotransport measurements in the WTe_2 system (sample 1). Normalized magnetoresistivity $\rho(H)/\rho(0)$ of sample 1 measured in (b) the perpendicular field with $H \parallel c$ axis, and (c) the parallel field with $H \parallel b$ axis and (d) $H \parallel a$ axis at different temperatures, respectively.

increasing temperature, MR decreases and the SdH oscillations are totally suppressed above 15 K. The field dependences of MR in the parallel field ($H \parallel b$ axis) at different temperatures are plotted in Fig. 2(c). The MR at low temperatures shows a classic parabolic dependence on the magnetic field with SdH oscillations at high fields. Compared to the MR measured in the perpendicular field ($H \parallel c$ axis), the MR effect measured in the parallel field ($H \parallel b$ axis) is decreased to $9 \times 10^4\%$ at 14.7 T at 2 K. Unexpectedly, when the magnetic field is parallel to the applied current along the a axis, the MR shows a quite linear behavior rather than a parabolic behavior [Fig. 2(d)]. Even still, the linear MR is as large as 1200% at $T = 2$ K and $\mu_0 H = 15$ T without any saturated trend. Moreover, the LMR property survives up to 50 K when temperature is increased. A detailed analysis on the SdH oscillations is given in the Supplemental Material [20].

To further investigate the Fermi surface of WTe_2, it is necessary to measure the angular-dependent MR behavior. Figure 3(a) shows MR behavior in a rotation by varying the relative magnetic field direction from the c axis to the b axis. The MR effect as well as the SdH oscillation is gradually weakened when rotating the magnetic field orientation away from the c axis. Figure 3(b) demonstrates how the MR behavior changes in a rotation when the magnetic field is varied from the b axis ($H \perp I$) to the a axis ($H \parallel I$). While MR is quadratically dependent on the magnetic field when $H \parallel b$ axis (0°), it deviates as H is rotated away from the b axis. When $H \parallel I \parallel a$ axis, the MR exhibits a nonsaturating but linear behavior, showing an extremely anisotropic characteristic of WTe_2.

To better understand the angular-dependent MR in WTe_2, we performed transport measurements to investigate the tilting-angle dependence of MR at 2 K at different magnetic fields [Figs. 3(c) and 3(d)]. As shown in Fig. 3(c), the observed angular dependence of MR in WTe_2 can be fitted by the $|\cos\theta|$ function, where θ is the angle between the magnetic field and the c axis of WTe_2. Moreover, when the magnetic field is tuned from the b axis to the a axis, the MR also shows obvious oscillations. These prominent MR oscillations with the function form $|\cos\theta|$ indicate significant anisotropy of the carrier in the semimetal WTe_2. Furthermore, the additional angular-dependent MR oscillations are observed at high magnetic fields when the field rotates in the cb plane [Fig. 3(c)], which is absent in the rotation case in the ab plane [Fig. 3(d)]. When the magnetic field is lower than 6 T, the additional oscillations disappear, which is consistent with the observed SdH oscillations in WTe_2.

To further reveal the anisotropic MR features in WTe_2, we measured sample 2 with a size of ~1.2 mm × 0.29 mm × 25 μm (length × width × thickness) from the same batch with the current applied along the b axis ($I \parallel b$ axis). The MR properties of sample 2 under different magnetic field directions are shown in Figs. 4(a)–4(c). When the current is applied along the b axis, the sample always displays classical quadratic MR for three different orientations of the magnetic field ($H \parallel c$ axis, $H \parallel b$ axis, and $H \parallel a$ axis). The longitudinal LMR observed in Fig. 2(d) has disappeared. It demonstrates that the LMR feature is related to the crystal direction. Additionally, as shown in Fig. 4(d), the angular-dependent MR behavior also

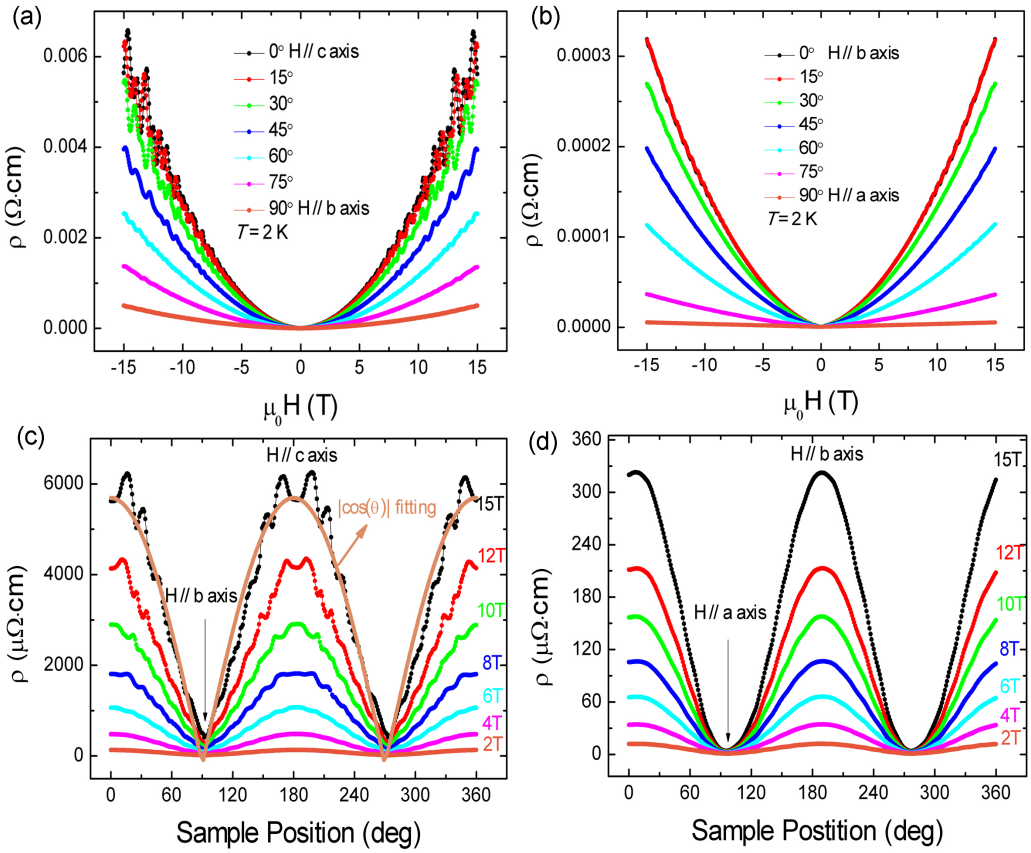

FIG. 3. (Color online) (a) Field-dependent magnetoresistivity in sample 1 at $T = 2$ K with the magnetic field rotating from the c axis (0°) to the b axis (90°). (b) Magnetoresistivity in sample 1 measured at different angles in the ab plane at $T = 2$ K. (c), (d) Magnetoresistivity in sample 1 as a function of tilt angle in different magnetic fields at $T = 2$ K for the field rotating in the cb plane and ab plane, respectively. The function $|\cos\theta|$ fitting is shown as a solid dark orange curve in (c).

shows distinct MR oscillations with the function form $|\cos\theta|$, similar to the behavior observed in Fig. 3(d), suggesting the anisotropy of the carrier in WTe_2 is independent of the applied current direction.

In order to confirm the exotic LMR in WTe_2 (when $H \parallel I \parallel a$ axis) is related to the crystal orientation, we also measured the MR behavior of sample 2 when the current is applied along the a axis. The temperature dependences of resistivity of sample 2 for current along the a and b axes are shown in Fig. 5(a). An expanded version of the low temperature regime is shown in the inset. It is clear that an obvious anisotropic behavior of resistivity can be observed in both the high and low temperature regions. Figure 5(b) displays the MR behavior in the perpendicular field ($H \parallel c$ axis) when the current is parallel to the a axis. The MR effect is 1.1×10^5% at 15 T at 2 K, which is about three times larger than the MR measured when $I \parallel b$ axis [Fig. 4(a)], indicating an anisotropic MR behavior. In order to explore the exotic longitudinal LMR behavior, the detailed orientation-dependent MR behavior around the a axis is shown in Fig. 5(c). When the magnetic field is parallel to the a axis, a perfect LMR is observed [inset of Fig. 5(c)], however, it changes to parabolic as H rotates away from the a axis. The exotic LMR behavior may closely relate to the unique one-dimensional tungsten chain (a axis). Nevertheless, further studies are needed to reveal the microscopic origin of the exotic LMR feature. Figure 5(d) displays the field dependence of MR at 2 K with the relative magnetic field rotating along from the c axis (0°) to the a axis (90°). It implies that the anisotropic behavior is general in the WTe_2 system, regardless of the applied current direction.

In short, the transport property of the WTe_2 system shows three distinct features: (i) a remarkable anisotropic resistivity and anisotropic MR when tuning the magnetic orientation; (ii) the violation of Kohler's law for MR behavior measured in the perpendicular field when $I \parallel a$ axis; and (iii) an exotic large LMR when the magnetic field is parallel to the applied current direction along the a axis.

Previously, it has been reported that WTe_2 possesses a large, quadratic, nonsaturating MR [11], due to the compensation of the electron and hole carriers in the system [24]. Here, besides the nonsaturating MR, we also observed profound anisotropic transport features. Specifically, the anisotropic resistivity along the a and b axes in Fig. 5(a) indicates that the effective mass of the carrier satisfies $m_a \ll m_b$. Moreover, as shown in Figs. 2(a) and 2(b), when $I \parallel a$ axis, the MR measured when $H \parallel c$ axis is an order of magnitude larger than that for $H \parallel b$ axis, indicating the effective mass $m_b \ll m_c$. These anisotropic effective masses of the carrier can give rise to MR oscillations with the function form $|\cos\theta|$ [shown in Figs. 3(c), 3(d), 4(d), and Fig. 5(d)]. Additionally,

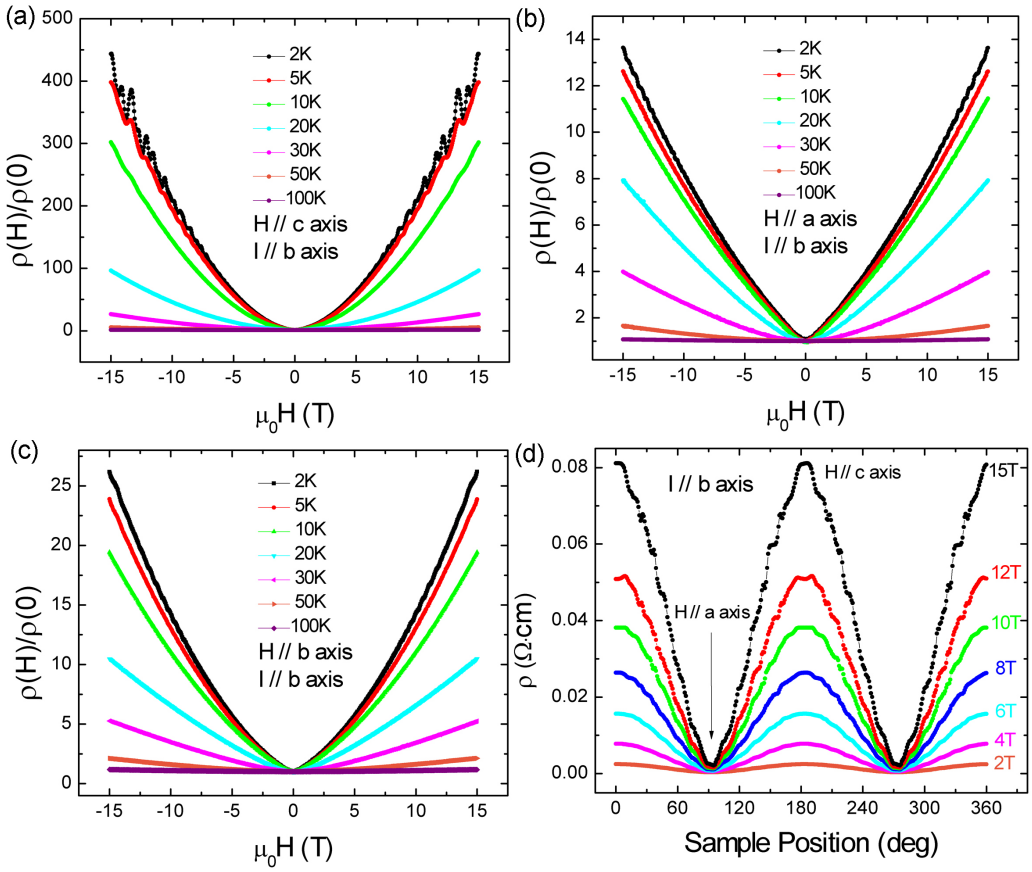

FIG. 4. (Color online) Normalized magnetoresistivity in sample 2 with (a) the perpendicular field with $H \parallel c$ axis, and (b) the parallel field with $H \parallel a$ axis and (c) $H \parallel b$ axis at different temperatures, respectively. (d) Field-dependent magnetoresistivity at $T = 2$ K with the magnetic field rotating from the c axis (0°) to the a axis (90°). The current is along the b axis.

a recent angle-resolved photoemission spectroscopy (ARPES) experiment demonstrated the complicated Fermi surface along the $\Gamma - X$ lines [25], supporting the scenario of an anisotropic mass of the carrier in WTe_2.

Next, we turn to the observed violation of Kohler's law for the MR measured in the perpendicular field when $I \parallel a$ axis. In the large field limit with $\mu(T)B \gg 1$, the MR can be written as [24]

$$\frac{\Delta\rho(\mu_0 H,T)}{\rho_0(T)} = [\mu(T)\mu_0 H]^2 = \left[\frac{\mu_0 H}{n(T)e\rho_0(T)}\right]^2,$$

with $\mu(T)$ and $n(T)$ denoting the mobility and total carrier density at temperature T. Commonly, the carrier density $n(T)$ is not sensitive to the change in temperature, which results in the Kohler's rule [24]. However, in WTe_2 with electron and hole carriers, the formation of excitons can change the carrier density, which leads to the violation of Kohler's rule, similar to other correlated systems [26]. As shown in Fig. 1(d), the slope of the scaling plot of MR first increases and then decreases around 20 K with increasing temperature. This behavior indicates that the carrier density may also nonmonotonically depend on the temperature—first decreasing then increasing. In the WTe_2 single crystal, the electron and hole pockets lie separately along the Γ-X line. The formation of excitons in three-dimensional systems needs perfect nesting of the electron and hole pockets, which can hardly be satisfied due to the different shapes of the electron and hole Fermi surfaces. With increasing temperature, a phonon with wave vector $\vec{k}_0$ and frequency $\omega(\vec{k}_0)$ appears, and connects the electron and hole pockets. This typical phonon mode can promote the formation of excitons, which leads to the carrier density decreasing with increasing temperature. This formation of excitons is similar to the liquid-gas transition in previous studies [27,28]. We find the phonon energy for $\omega(\vec{k}_0)$ lies in the range of 10−20 K (see the Supplemental Material [20]). With increasing temperature, thermal activation can destroy the excitons for temperatures larger than the excitonic gap, resulting in an increase in the carrier density for higher temperatures. Overall, the phonons assist exciton formation, and thermal activation destroys the excitons. These double effects can give rise to the nonmonotonic carrier density dependence on temperature and may result in a minimum charge carrier density around 20 K.

Third, we consider the origin of exotic large LMR when $H \parallel I \parallel a$ axis at low temperatures. Classically, the resistance has no response to an external magnetic field applied parallel to the excitation current. However, the quantum effect gives rise to Landau levels accompanied with quasi-one-dimensional (1D) dispersion along the magnetic field. In the quantum limit, the large degeneracy of Landau levels leads to correlated effects.

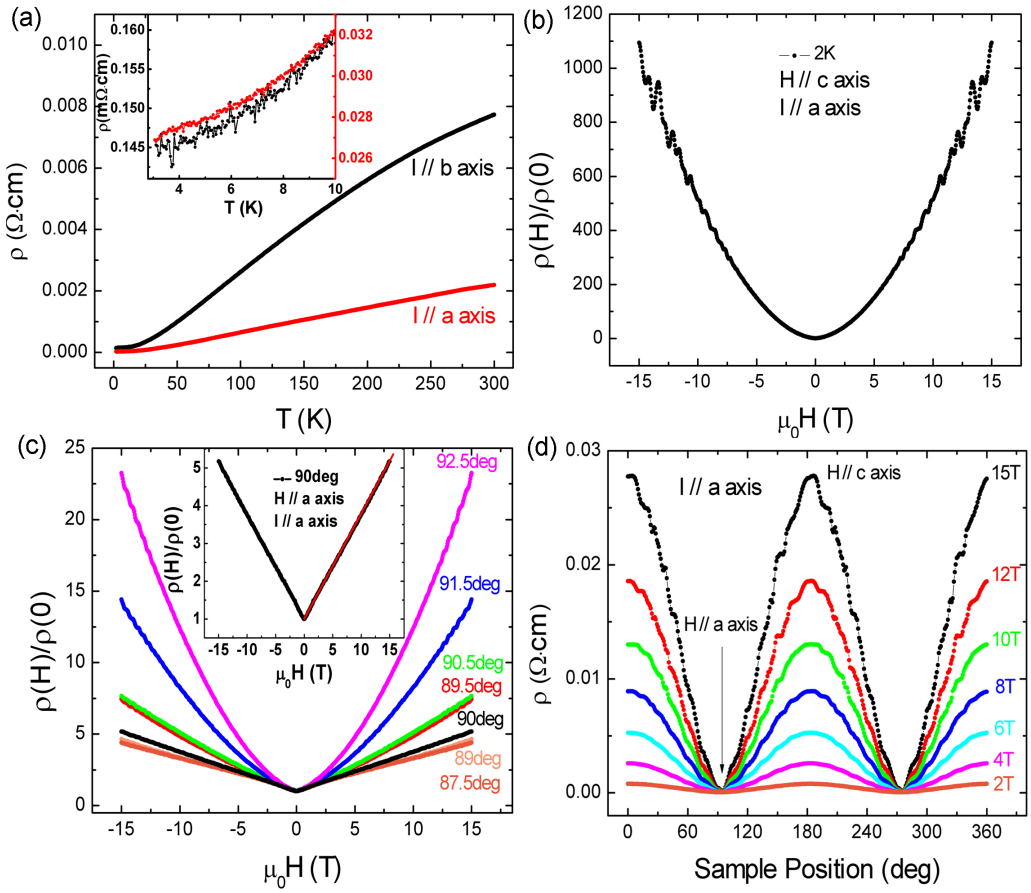

FIG. 5. (Color online) (a) Temperature dependence of resistivity in sample 2 for current along the a or b axis, respectively. The inset shows the expanded low temperature region. (b) shows the normalized magnetoresistivity in sample 2 for current along the a axis in the perpendicular field ($H \parallel c$ axis). A detailed orientation dependence is shown in (c) for H around the a axis. The inset shows the LMR behavior when H is parallel to the a axis. The red solid curve is linear fitting. (d) Field-dependent magnetoresistivity at $T = 2\,\mathrm{K}$ with the magnetic field rotating from the c axis (0°) to the a axis (90°). The current is along the a axis.

A well-known example is the charge density wave instability in bismuth in the quantum limit [29,30]. Especially in WTe_2, the system has an equal number of electron and hole carriers. The magnetic field $H \parallel a$ axis leads to quasi-1D electron and hole states along the Γ-X line, and the density for each quasi-1D states satisfies $dN(n,k_x)/dk_x = eB/2\pi hc$. The scattering between electronlike and holelike Landau levels significantly increases with increasing magnetic field, and contributes to the observed large LMR. Further study is expected to uncover the scattering and the exciton formation in this correlated, compensated carrier system.

In summary, intriguing quantum transport properties of WTe_2 are revealed by systematic angle-dependent MR measurements at different temperatures. A large RRR in zero field and a metal-insulator transition driven by the perpendicular field are observed. More interestingly, the MR of WTe_2 shows extremely anisotropic properties. The parabolic MR reaches as high as $1.1322 \times 10^6\%$ at 14.7 T at 2 K when $H \parallel c$ axis but decreases to $9 \times 10^4\%$ when $H \parallel b$ axis. Surprisingly, an exotic large LMR as high as 1200% at 15 T is observed when $H \parallel I \parallel a$ axis. An empirical model of a double carrier correlated system is developed based on the balanced hole-electron condition in WTe_2 to explain the observations. We expect that our research will encourage further theoretical and experimental studies on this exciting double carrier correlated layered material and its corresponding quantum properties.

Note added: We note the recent two papers for anisotropic properties of WTe_2 crystals [31,32].

We acknowledge Qian Niu, Fa Wang, and Hua Chen for helpful discussions. This work was financially supported by the National Basic Research Program of China (Grants No. 2013CB934600 and No. 2012CB921300), the National Natural Science Foundation of China (No. 11222434 and No. 11174007), and the Research Fund for the Doctoral Program of Higher Education (RFDP) of China. D.G.M. acknowledges support from the Gordon and Betty Moore Foundation's EPiQS Initiative through Grant No. GBMF4416. J.Q.Y. acknowledges support from the U.S. Department of Energy, Office of Science, Basic Energy Sciences, Materials Sciences and Engineering Division. Y.W. acknowledges support from the Natural Science Foundation of China (11174244) and Zhejiang Provincial Natural Science Foundation of China (LR12A04002).

Y.Z. and H.L. contributed equally to this work.

[1] R. Xu, A. Husmann, T. F. Rosenbaum, M.-L. Saboungi, J. E. Enderby, and P. B. Littlewood, Nature (London) **390**, 57 (1997).
[2] A. L. Friedman, J. L. Tedesco, P. M. Campbell, J. C. Culbertson, E. Aifer, F. K. Perkins, R. L. Myers-Ward, J. K. Hite, C. R. Eddy, Jr., G. G. Jernigan, and D. K. Gaskill, Nano Lett. **10**, 3962 (2010).
[3] H. Tang, D. Liang, R. L. Qiu, and X. P. Gao, ACS Nano **5**, 7510 (2011).
[4] X. Wang, Y. Du, S. Dou, and C. Zhang, Phys. Rev. Lett. **108**, 266806 (2012).
[5] Y. Zhao, C.-Z. Chang, Y. Jiang, A. DaSilva, Y. Sun, H. Wang, Y. Xing, Y. Wang, K. He, X. Ma, Q.-K. Xue, and J. Wang, Sci. Rep. **3**, 3060 (2013).
[6] L. Tian, Q. Gibson, M. N. Ali, M. Liu, R. J. Cava, and N. P. Ong, Nat. Mater. **14**, 280 (2014).
[7] Y. Zhao, H. Liu, C. Zhang, H. Wang, J. Wang, Z. Lin, Y. Xing, H. Lu, J. Liu, Y. Wang, S. Jia, X. C. Xie, and J. Wang, arXiv:1412.0330.
[8] A. Narayanan, M. D. Watson, S. F. Blake, N. Bruyant, L. Drigo, Y. L. Chen, D. Prabhakaran, B. Yan, C. Felser, T. Kong, P. C. Canfield, and A. I. Coldea, Phys. Rev. Lett. **114**, 117201 (2015).
[9] M. Novak, S. Sasaki, K. Segawa, and Y. Ando, Phys. Rev. B **91**, 041203 (2015).
[10] A. A. Abrikosov, Phys. Rev. B **58**, 2788 (1998).
[11] M. N. Ali, J. Xiong, S. Flynn, J. Tao, Q. D. Gibson, L. M. Schoop, T. Liang, N. Haldolaarachchige, M. Hirschberger, N. P. Ong, and R. J. Cava, Nature (London) **514**, 205 (2014).
[12] I. Pletikosić, M. N. Ali, A. V. Fedorov, R. J. Cava, and T. Valla, Phys. Rev. Lett. **113**, 216601 (2014).
[13] H. Y. Lv, W. J. Lu, D. F. Shao, S. G. Tan, and Y. P. Sun, Europhys. Lett. **110**, 37004 (2015).
[14] P. L. Cai, L. P. He, J. Pan, X. C. Hong, Z. Zhang, J. Wei, Z. Q. Mao, and S. Y. Li, arXiv:1412.8298.
[15] X.-C. Pan, X. Chen, H. Liu, Y. Feng, Z. Wei, Y. Zhou, Z. Chi, L. Pi, F. Yen, F. Song, X. Wan, Z. Yang, B. Wang, G. Wang, Y. Zhang, arXiv:1501.07394.
[16] D. Kang, Y. Zhou, W. Yi, C. Yang, J. Guo, Y. Shi, S. Zhang, Z. Wang, C. Zhang, S. Jiang, A. Li, K. Yang, Q. Wu, G. Zhang, L. Sun, and Z. Zhao, arXiv:1502.00493.
[17] X. Qian, J. Liu, L. Fu, and J. Li, Science **346**, 1344 (2014).
[18] W. G. Dawson and D. W. Bullett, J. Phys.: Condens. Matter **20**, 6159 (1987).
[19] J. Augustin, V. Eyert, Th. Böker, W. Frentrup, H. Dwelk, C. Janowitz, and R. Manzke, Phys. Rev. B **62**, 10812 (2000).
[20] See Supplemental Material at http://link.aps.org/supplemental/10.1103/PhysRevB.92.041104 for detailed analysis of transport data as well as the first-principles calculation on the band structure of WTe_2 crystal.
[21] P. L. Kapitza, Proc. R. Soc. London, Ser. A **119**, 358 (1928).
[22] K. Wang, D. Graf, L. Li, L. Wang, and C. Petrovic, Sci. Rep. **4**, 7328 (2014).
[23] X. Du, S.-W. Tsai, D. L. Maslov, and A. F. Hebard, Phys. Rev. Lett. **94**, 166601 (2005).
[24] J. M. Ziman, *Electrons and Phonons: The Theory of Transport Phenomena in Solids* (Clarendon, Oxford, UK, 2001).
[25] J. Jiang, F. Tang, X. C. Pan, H. M. Liu, X. H. Niu, Y. X. Wang, D. F. Xu, H. F. Yang, B. P. Xie, F. Q. Song, X. G.Wan, and D. L. Feng, arXiv:1503.01422.
[26] N. Luo and G. H. Miley, Physica C: Superconductivity **371**, 259 (2002).
[27] W. F. Brinkman and T. M. Rice, Phys. Rev. B **7**, 1508 (1973).
[28] S. He and X. C. Xie, Phys. Rev. Lett. **80**, 3324 (1998); J. Shi and X. C. Xie, *ibid.* **88**, 086401 (2002).
[29] D. Yoshioka and H. Fukuyama, J. Phys. Soc. Jpn. **50**, 725 (1981).
[30] V. M. Yakovenko, Phys. Rev. B **47**, 8851 (1993).
[31] Z. Zhu, X. Lin, J. Liu, B. Fauqué, Q. Tao, C. Yang, Y. Shi, and K. Behnia, Phys. Rev. Lett. **114**, 176601 (2015).
[32] L. R. Thoutam, Y. L. Wang, Z. L. Xiao, S. Das, A. Luican-Mayer, R. Divan, G. W. Crabtree, and W. K. Kwok, arXiv:1506.02214 [Phys. Rev. Lett. (to be published)].